

Quarter-filled Kane-Mele Hubbard model: Dirac half-metals

S. Mellaerts¹, R. Meng¹, V. Afanasiev¹, J.W. Seo², M. Houssa^{1,3} and J.-P. Locquet¹

¹*Department of Physics and Astronomy, KU Leuven, Celestijnenlaan 200D,
3001 Leuven, Belgium,* ²*Department of Materials Engineering,
KU Leuven, Kasteelpark Arenberg 44, 3001 Leuven,
Belgium,* ³*Imec, Kapeldreef 75, 3001 Leuven, Belgium**

Recent experimental success in the realization of two-dimensional (2D) magnetism has stimulated the search for new magnetic 2D materials with strong magnetic anisotropy and high Curie temperature. One promising subgroup of 2D magnetic systems are Dirac half-metals (DHM) which have gained a lot of interest recently, as they host a high-temperature quantum anomalous Hall effect (QAHE). This article discusses predictions for intrinsic DHMs and identifies them as realizations of the Kane-Mele Hubbard model at quarter filling. This proposed unification contributes to a firmer understanding of these materials and suggests pathways for the discovery of new DHM systems.

I. INTRODUCTION

The realization of magnetic semiconductors at room-temperature for spintronic applications remains one of the biggest challenges in material physics. Recently there have been many first-principle studies searching to identify a magnetic semiconducting phase in two-dimensional (2D) systems, including the prediction of various new concepts and materials, such as spin-gapless semiconductors (SGS). The first SGS was proposed by Wang [1] in 2008 and can be considered as a material being gapless in one spin channel and semiconducting/insulating in the other. A distinction must be made between a parabolic and a linear dispersion in the gapless spin channel, where the latter case leads to a Dirac cone in one spin channel and materials which are often called Dirac spin-gapless semiconductor (DSGS).

Importantly, as pointed out by Wang *et al.* [2], there exists a difference between a DHM and DSGS. In both cases there is a Dirac cone in one spin channel and a gap in the other, but in the former case the Dirac cone is not necessarily located at the Fermi level. However for convenience in this paper, we shall refer to these together as the general group of DHMs. Furthermore, the group of DHMs is further divided into *p*- and *d*-state DHMs, which refers to the orbitals involved in the Dirac state. This work will mainly focus on the intrinsic materials with *d*-state Dirac half-metallicity.

Since the first theoretical prediction of a DHM in a triangular ferrimagnet [3] there have been many other suggestions of DHMs based on first-principle calculations. For instance, the transition-metal (TM) trihalides monolayers have been considered as an excellent system for the realization of these DHM phases that all host a QAHE [4–8]. Moreover, V-group TM sesquichalcogenide with a honeycomb-kagome (HK) lattice have also been predicted to achieve a DHM phase with room-temperature QAHE [9–11]. However, a firm theoretical framework of

these DHMs and the room-temperature QAHE in these systems is still lacking.

In this paper, we provide a theoretical framework based on the Kane-Mele Hubbard (KMH) model that unifies the various predictions of DHMs, with some of them hosting a room-temperature magnetic Chern insulator by the existence of an atomic on-site spin-orbit coupling (SOC). Furthermore, we discuss the universal features of these DHMs, where we elucidate the importance of their multi-orbital structure.

II. KANE-MELE HUBBARD MODEL

As the quantum spin Hall effect (QSHE) in graphene and other 2D Xenos (e.g. silicene) can be described by the Kane-Mele model [12], we argue that the realization of DHMs hosting a QAHE can be captured by the inclusion of the electron correlations into the Kane-Mele model - the KMH model - described by the hamiltonian

$$\begin{aligned}
 H = & -t \sum_{\langle ij \rangle, \alpha} \left(c_{i\alpha}^\dagger c_{j\alpha} + h.c. \right) \\
 & - i\lambda_{SO} \sum_{\langle\langle ij \rangle\rangle, \sigma} \left(c_{i\alpha}^\dagger \nu_{ij} \sigma_{\alpha\beta}^z c_{j\beta} + h.c. \right) \\
 & + U \sum_i n_{i\uparrow} n_{i\downarrow}
 \end{aligned} \tag{1}$$

where t is the hopping parameter, λ_{SO} the spin-orbit coupling parameter, U the Hubbard on-site parameter, $c_{i\alpha}^\dagger$ ($c_{i\alpha}$) the electron creation (annihilation) operator at site i with spin state $\alpha \in \{\uparrow, \downarrow\}$ on the honeycomb lattice, $n_{i\alpha}$ the number density operator, σ^z a Pauli matrix, $\langle ij \rangle$ and $\langle\langle ij \rangle\rangle$ denotes resp. nearest and next-nearest neighbour hopping, and $\nu_{ij} = \pm 1$ depending on whether the hopping path bends to the right or left.

This model has been studied intensively in the half-filled situation [13–15], however only a few studies ex-

* simon.mellaerts@kuleuven.be

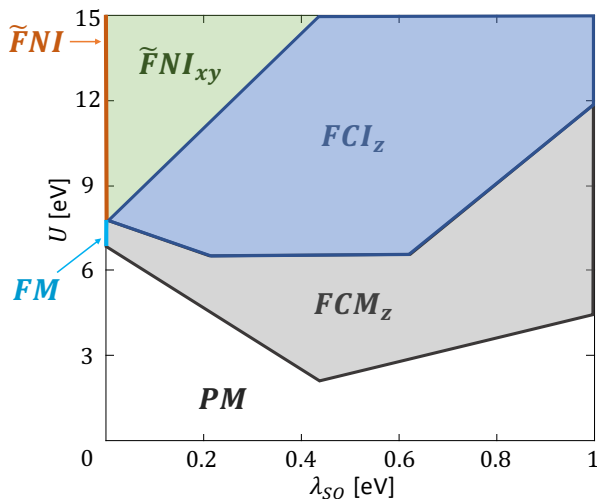


Figure 1. The simplified phase diagram of the Kane-Mele-Hubbard model at quarter filling on the honeycomb lattice where the hopping parameter is taken to be $t = 1$ eV, with the on-site Coulomb repulsion on the y -axis and on the x -axis the intrinsic SOC. The phases present in the phase diagram are: paramagnetic metal (PM), FM metal (FM), FM normal insulator (FNI), FM Chern metal (FCM), FM Chern insulator (FCI), and other related phases with F or \tilde{F} to indicate FM order with or without inversion symmetry and subscripts xy or z representing the direction of the magnetic order. Adapted from [16].

explored the case of quarter filling. Recently, this model was solved within the mean-field approximation and its phase diagram was obtained [16], shown simplified in Fig. 1. In the case of non-zero λ_{SO} and small U , the exchange splitting will not be sufficiently strong to establish a spin-polarized Dirac cone, and the eventual gap opening by SOC at the Dirac point will be closed by the overlapping of the spin-minority bands. Under those conditions a paramagnetic metal (PM) or ferromagnetic Chern metal phase (FCM_z) is stabilized. Upon further increasing U a magnetic Chern insulating phase (FCI_z) with strong magnetic anisotropy is established. This situation can be understood as the cooperative effect of strong U and λ_{SO} , where the former results in a large exchange splitting, whereas the latter provides the strong magnetic anisotropy [17] and opens a gap at the Dirac point. On further increasing U , a trivial Mott insulating phase (\tilde{FNI}_{xy}) with broken inversion symmetry will appear, however in contrast to a typical antiferromagnetic Mott insulator, an in-plane FM order is established as explained in [18].

III. UNIFICATION OF DHM

To our knowledge, the DHM phases hosting a QAHE can be divided into two classes: V-group TM

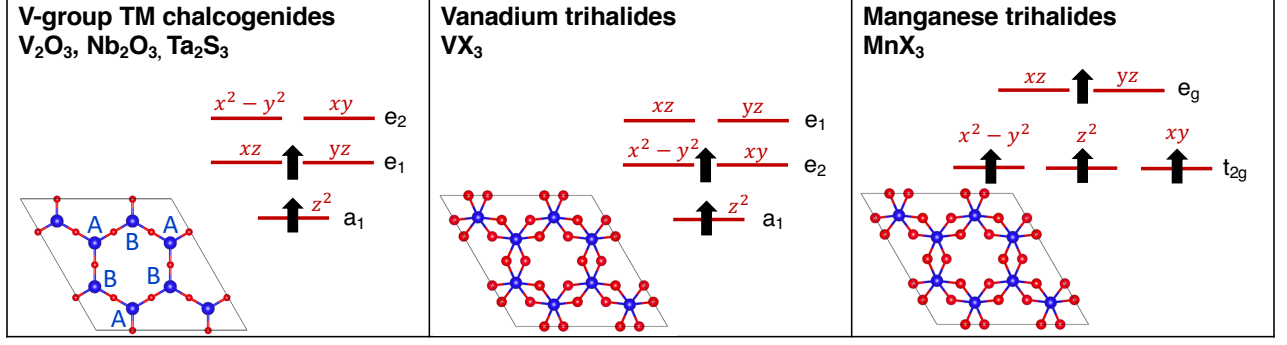
sesquichalcogenide monolayers with HK lattice structure and the honeycomb TM trihalide monolayers, with their respective lattice structure shown in Fig. 2(top). The former group can be further subdivided by its crystal field (CF) environment as either octahedral or distorted octahedral. This gives rise to three types of CF splitting situations, as illustrated in Fig. 2(top). In all these situations the TM forms a honeycomb structure, which is crucial for the existence of a Dirac cone [19].

The most simple realization of quarter filling of the d orbital levels is the situation of strong U , where exchange splitting between the spin-majority and minority channels is sufficiently large such that only one spin channel remains close to the Fermi level. For the distorted octahedral case, two remaining electrons on the TM ion after bonding with the halide gives rise to quarter filling of the e_2 orbital level, which is realized in VBr_3 [4] due to the two-fold degeneracy of this ($d_{xy}, d_{x^2-y^2}$) level. In the case of octahedral CF splitting, there would be quarter filling of e_g for four remaining electrons on the TM ion, which happens for MnX_3 with $X = F, Cl, Br, I$ [6]. Finally, in the HK M_2X_3 with trigonal CF there will be a quarter filled e_1 orbital when there are two remaining electrons on the TM ion after bonding with the chalcogenides. This situation has been established in V_2O_3 [9], Ta_2S_3 [11] and Nb_2O_3 [10]. All of the above mentioned systems have been predicted to be a DHM phase hosting QAHE. These situations can be understood as the realization of the Haldane model, where the strong U and SOC result in the formation of a strong magnetic moment which destroys one spin channel of the Kane-Mele model, leaving one QAH state.

These are the most trivial situations that confirm part of the phase diagram in Fig. 1. However, this KMH tight-binding (TB) model does not take into account the multi-orbital level nature of these compounds, which allows the realization of many more situations where the combination of CF splitting and exchange splitting allows the quarter filling of the orbital levels at much lower U . In this way, TM with higher electron occupation of the d -orbitals can also stabilize a DHM phase. For example, $NiCl_3$ [5], $PtBr_3$ and $PdBr_3$ [7] where the $4d$ and $5d$ have a slightly lower U but where the strong CF splitting allows the situation of six remaining electrons to fill the t_{2g} level and one remaining electron that leads to quarter filling of the e_g level, as illustrated at the bottom of Fig. 2. Moreover, due to the presence of particle-hole symmetry, the realization of a three-quarter filled d -orbital is equivalent. This situation was predicted in iron trihalides FeX_3 [8]. Again these type of systems have also been predicted to be DHM phases with a SOC-induced QAHE.

Furthermore, some of these systems (e.g. VBr_3 and FeX_3) have also been predicted to become a Mott insulator by including a sufficiently large U (> 0.5 eV). We relate these systems to the KMH model by arguing that the quarter-filled orbital level consists of the in-

Trivial cases: Strong spin polarization



Non-trivial cases: Cooperation of CF and exchange splitting

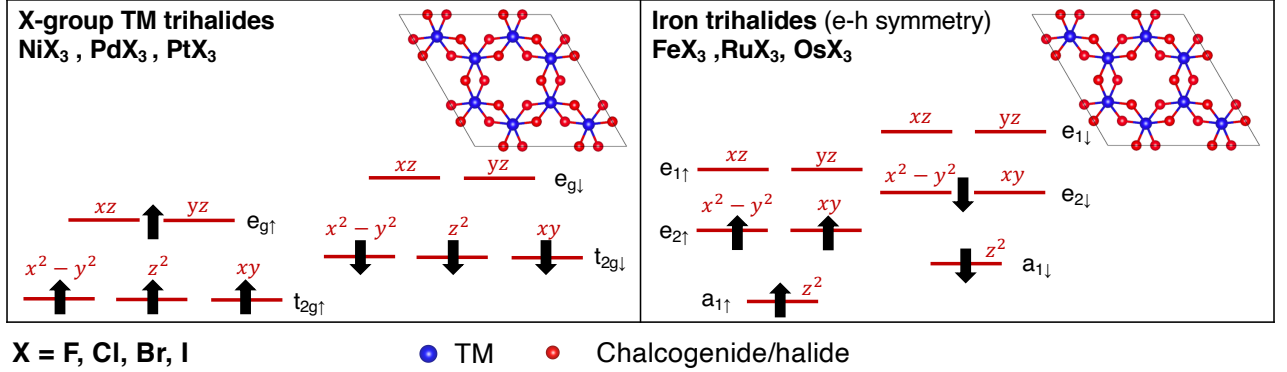


Figure 2. Unification scheme of the Dirac half-metals based on the quarter-filled KMH model. The lattice structure (with sublattices $\tau = A, B$) for each realization of quarter-filled d -orbital level is depicted with the blue atoms representing the TM and the red atoms the chalcogenides/halides. The unification scheme is further divided by trivial cases where a strong U results in a strong exchange splitting, whereas in the non-trivial cases there is the cooperation of a CF and exchange splitting to satisfy the quarter-filled level condition.

plane ($d_{xy}, d_{x^2-y^2}$) orbitals, which will have a larger overlap leading to a larger hopping term t . Consequently, rescaling the phase diagram by t should make the Mott insulating phase ($\tilde{F}NI_{xy}$) accessible at lower U .

The various realizations of the quarter-filled KMH model are summarized in Fig. 2, which are all predicted to be DHMs hosting a QAHE. They can be classified according to a scheme where quarter-filling of the d -orbital level is established. Identifying this crucial ingredient of quarter-filling provides the opportunity to search for other DHMs. For example, we expect that materials with TM and halide/chalcogenide in the same chemical group can also yield the same quarter-filled orbitals. Nevertheless, this does not mean that this quarter-filled KMH model is inclusive in the sense that all intrinsic d -state DHMs should be the realization of this model. Moreover, this simple TB model has also certain shortcomings. The most important one is the prediction of the magnetic ground state and magnetic anisotropy where CF splitting, orbital orientations and exchange interactions are critical and the TB model might not capture these accurately. Nonetheless, as will be shown in Sec. IV this model gives insights on how the cooperative effect of SOC

and electron correlations can stabilize high-temperature magnetic Chern insulators.

IV. UNIVERSAL FEATURES OF DHMS

In this section, a more detailed study of the low energy physics and the realized QAHE is given. We identify the common features and unify them within a TB model adopted in earlier studies on the (p_x, p_y) honeycomb lattice systems [20, 21]. Before discussing the universal features, it is also important to make a further distinction between two systems within the unification scheme in Fig. 2, depending on the type of quarter-filled degenerate orbital levels involved. In the case of quarter-filled (d_{xz}, d_{yz})-orbitals, there will be a π -bond between the TMs with only a small orbital overlap and thus small hybridization with the p -orbitals of the chalcogenides/halides. In this case, it can be expected that a TB model will be fairly accurate capturing most of the features. However, in the other case of quarter-filled ($d_{xy}, d_{x^2-y^2}$)-orbitals, a strong in-plane hybridization with the ligand orbitals is expected, making a TB

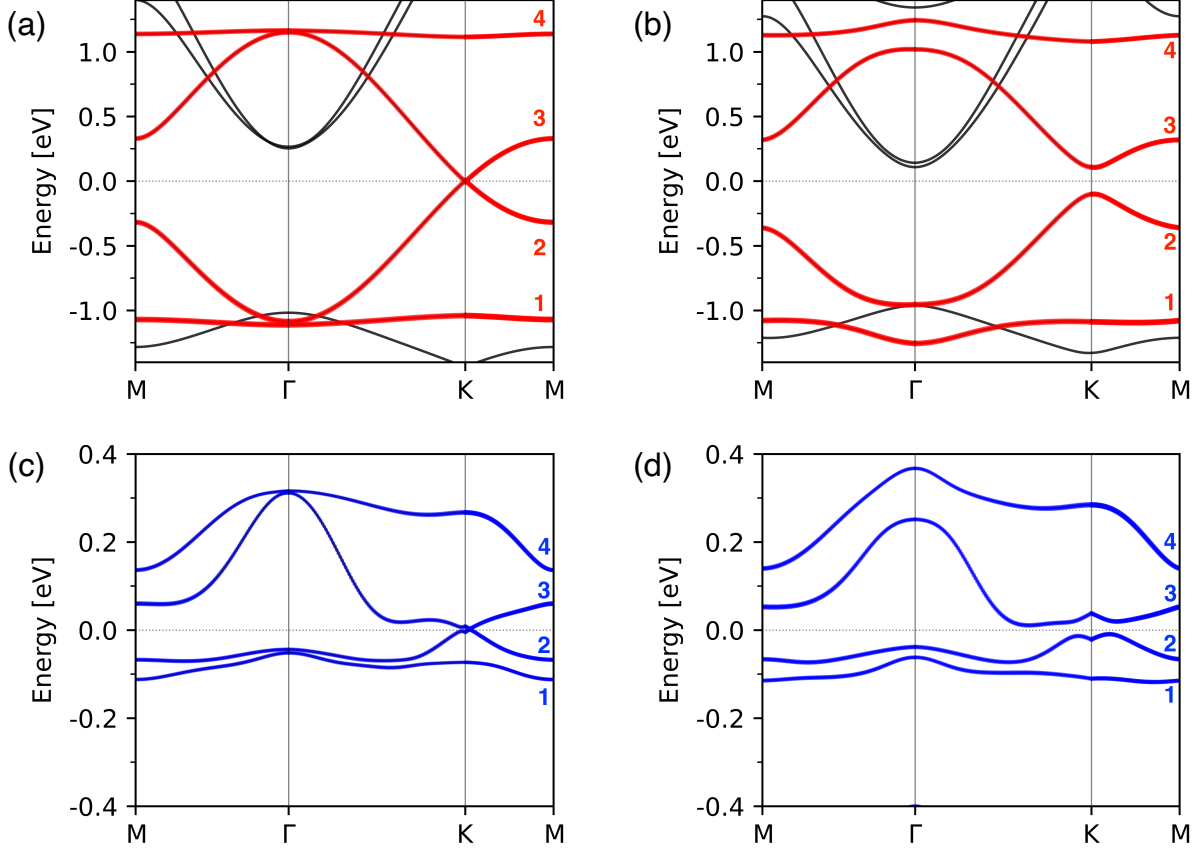


Figure 3. The DFT calculated band structure of DHMs with the four low-energy bands indicated by red/blue. The band structure of (a-b) V₂O₃ and (c-d) MnBr₃ without and with SOC respectively.

approach a less appropriate description.

A. Topological band structure

The two-fold degenerate d -orbitals that are quarter-filled will be responsible for the low-energy physics of the system. The two-fold degeneracy of the orbitals together with the sublattice symmetry gives rise to a total of four bands close to the Fermi level E_F , as shown in Fig. 3. Two bands are dispersive and form a Dirac cone at the K (K') point (band 2 and 3), while the other two bands are (nearly-)flat (band 1 and 4) forming a degeneracy with the dispersive bands at the Γ point. As examples of the low-energy band structures of TM sesquichalcogenide and TM trihalides, the band structure of resp. V₂O₃ and MnBr₃ are shown in Fig. 3. These band structures were calculated by density functional theory (DFT) (See Supplemental Material).

This four-band low-energy physics of the DHMs is very similar to the low-energy physics of the (p_x, p_y) -orbital honeycomb lattice which has been studied intensively in the context of ultracold-atom optical lattices [22–24].

Therefore, these TB calculations and their results can be used for the description of these DHM phases. Here, only the main results of this four-band model are formulated, the full calculation can be found in [21]. Neglecting the spin degree of freedom, a four-component basis can be constructed,

$$\psi_{\tau\sigma} = (d_{A,+}, d_{B,+}, d_{A,-}, d_{B,-}) \quad (2)$$

with $d_{\tau,\pm}^\dagger = \frac{1}{\sqrt{2}}(d_{\tau,xz}^\dagger \pm id_{\tau,yz}^\dagger)$ or $d_{\tau,\pm}^\dagger = \frac{1}{\sqrt{2}}(d_{\tau,xy}^\dagger \pm id_{\tau,x^2-y^2}^\dagger)$ the orbital angular momentum L_z eigenstates with resp. eigenvalues $L_z = \pm 1$ and $L_z = \pm 2$, and with sublattice component $\tau = A, B$. In other words, the doublet of orbital angular momentum and the sublattice structure give rise to two pseudospin degrees of freedom, which are only conserved at certain high-symmetry points. For simplicity, we will restrict the discussion to the case of a four-band model for the orbital angular momentum eigenstates $d_{\tau,\pm} = \frac{1}{\sqrt{2}}(d_{\tau,xz} \pm id_{\tau,yz})$ with $L_z = \pm 1$. However, this discussion can be easily generalized to the other situation with $L_z = \pm 2$.

At the K point, the eigenstates of the two middle bands are orbital eigenstates with $L_z = \pm 1$ where the spin-conserving on-site SOC will lift this orbital degeneracy, opening an energy gap equal to the eigenenergy difference between the SOC term $s_z L_z$ with $L_z = \pm 1$. As a result, the eigenstate of the band 2 will be the orbital eigenstate $d_{xz} + id_{yz}$ with $L_z = +1$ and eigenenergy $-\lambda_{SO}$ whose wave function is completely located on the B sublattice, while band 3 has orbital eigenstate $d_{xz} - id_{yz}$ with $L_z = -1$ and eigenenergy $+\lambda_{SO}$ completely located on sublattice A . Hence, the on-site SOC opens a topologically non-trivial energy gap of $2\lambda_{SO}$ in the presence of sublattice symmetry. This analysis can be easily generalized to the K' point.

On the other hand, at the Γ point, the hamiltonian $H(k)$ preserves all rotation symmetries i.e. the SOC term $s_z L_z$ commutes with $H(k)$. Consequently, the bands near the Γ point will have eigenstates which are the superposition of wave functions located on both A and B sublattices. Nonetheless, band 1 has orbital eigenstate with $L_z = -1$, while the eigenstate of band 2 is an $L_z = +1$ eigenstate. Therefore, similar to the K (K') points, the on-site SOC opens a non-trivial energy gap equal to the eigenenergy difference of the SOC term, $2\lambda_{SO}$. The topological nature of this gap opening at Γ away from E_F has been largely unrecognized in first-principles calculations.

B. Large energy gap and cooperation of U and SOC

The realization of the QAHE in DHMs arises from the cooperative effect of strong electron correlations and SOC, as stated in many first-principles studies on DHMs. However, the true origin of this relatively large energy gaps remains not well understood. Two excellent theoretical studies on (p_x, p_y) honeycomb lattice systems have clarified the observation of the large energy gaps opened by an intrinsic *atomic* SOC [20, 21]. In the literature, there have been two common mechanisms giving rise to topological band gaps: first the band inversion mechanism of two bands with different orbital character and second the next-nearest-neighbor (NNN) intrinsic SOC as in the Kane-Mele model. This latter mechanism, often at play in 2D topological materials, is typically a (second-order) NNN hopping process which only generates a relatively small energy gap. Therefore one seeks other topological materials where a sizeable SOC-induced gap can be found.

In graphene, the leading-order effective SOC is a second-order NNN process illustrated by the following sequence:

$$\begin{aligned} |p_{z\uparrow}^A\rangle &\xrightarrow{SOC} |p_{+\downarrow}^A\rangle \xrightarrow{V} |s_{\downarrow}^B\rangle \xrightarrow{V} |p_{+\downarrow}^A\rangle \xrightarrow{SOC} |p_{z\uparrow}^A\rangle \\ |p_{z\downarrow}^B\rangle &\xrightarrow{SOC} |p_{-\downarrow}^B\rangle \xrightarrow{V} |s_{\uparrow}^A\rangle \xrightarrow{V} |p_{-\downarrow}^B\rangle \xrightarrow{SOC} |p_{z\downarrow}^B\rangle \end{aligned} \quad (3)$$

with orbital angular momentum eigenstate $|p_{\pm}^{\tau}\rangle = p_x^{\tau} \pm ip_y^{\tau}$, *SOC* indicating the *intrinsic* atomic on-site SOC process, and V the nearest-neighbor direct hopping amplitude. This whole NNN hopping process involves an on-site SOC with two spin-flip $|p_{z\uparrow}^A\rangle \xrightarrow{SOC} |p_{\pm\downarrow}^A\rangle$ processes from the π -band to the σ -band, resulting in no net spin-flip effective SOC. As the intrinsic atomic SOC appears twice, the effective SOC will be a second-order process, making it a relatively weak effect. The importance of the multi-orbital nature became clear in the slightly larger SOC-induced gap opening in silicene and other Xenes [25–28], which have a low-buckled structure. In this case, the leading-order effective SOC is a first-order NNN process:

$$\begin{aligned} |p_{z\sigma}^A\rangle &\xrightarrow{V} |p_{-\sigma}^B\rangle \xrightarrow{\mp SOC} |p_{-\sigma}^B\rangle \xrightarrow{V} |p_{z\sigma}^A\rangle \\ |p_{z\sigma}^B\rangle &\xrightarrow{V} |p_{-\sigma}^A\rangle \xrightarrow{\pm SOC} |p_{-\sigma}^A\rangle \xrightarrow{V} |p_{z\sigma}^B\rangle \end{aligned} \quad (4)$$

where the low-buckled structure allows the coupling between the out-of-plane oriented p_z^A orbital and the in-plane oriented p_{\pm}^B orbitals. Hence, the electrons in p_z^A will hop to the nearest-neighbor p_{\pm}^B where they will experience the intrinsic atomic SOC, followed by a hopping to another nearest-neighbor p_z^A . Consequently, the effective SOC is a first-order NNN process, making it a slightly stronger effect when the buckling is sufficiently large to have a strong coupling (large V) between p_z^A and p_{\pm}^B .

The degenerate nature of the d -orbital levels in the DHM phases allows for the existence of an on-site atomic SOC without any nearest-neighbor hopping. In other words, the leading-order effective SOC processes are

$$\begin{aligned} |d_{\pm\uparrow}^{\tau}\rangle &\xrightarrow{\pm\lambda_{SO}} |d_{\pm\uparrow}^{\tau}\rangle \\ |d_{\pm\downarrow}^{\tau}\rangle &\xrightarrow{\mp\lambda_{SO}} |d_{\pm\downarrow}^{\tau}\rangle \end{aligned} \quad (5)$$

which are a first-order on-site processes. Intuitively we can think of a multi-orbital structure at each site allowing for intra-orbital hopping where the electrons will experience a strong atomic on-site SOC. Consequently, this atomic on-site SOC can result in large energy gap magnitudes (e.g. X -hydride/halide monolayer systems have energy gaps up to 0.65 eV [20]). Moreover, within the understanding of an energy gap opened by an atomic SOC, the cooperative behavior of the SOC and electron correlations (U) becomes evident; the Hubbard correction U will result in the localization of the electrons yielding a stronger atomic SOC effect. In terms of perturbation theory, U will force the orbital wave functions into more atomic-like wavefunctions over which the expectation value is taken when evaluating the SOC perturbation.

V. CONCLUSIONS

The obtained results provide a deeper understanding of a new type of DHM phases. We first unified the predictions of the intrinsic d -state DHMs by a simple TB model, the Kane-Mele Hubbard model at quarter filling. This identification provides a guide for the prediction of new DHMs, but also illustrates that DHMs might host many other phases under external conditions. In addition, some physical descriptions were given to obtain a better understanding on the cooperative effect of electron correlations and SOC. We elucidated the importance of the multiorbital structure for the existence of a strong on-site SOC and large energy gap, which is required for the room-temperature application of DHMs hosting a QAHE.

ACKNOWLEDGEMENTS

Part of this work was financially supported by the KU Leuven Research Funds, Project No. KAC24/18/056 and No. C14/17/080 as well as the Research Funds of the INTERREG-E-TEST Project (EMR113) and INTERREG-VL-NL-ETPATHFINDER Project (0559). Part of the computational resources and services used in this work were provided by the VSC (Flemish Super-

computer Center) funded by the Research Foundation Flanders (FWO) and the Flemish government.

SUPPLEMENTARY MATERIAL

All spin-polarized calculations were carried out within DFT, as implemented in Vienna *ab initio* simulation package (VASP) [29]. The generalized gradient approximation in the form of Perdew-Burke-Ernzerhof (PBE) [30] was used as exchange-correlation functional. The interactions between the electrons and ions were described by the projected-augmented-wave (PAW) pseudopotentials [31], and an energy cutoff of 550 eV was adopted. For the structural relaxation, a force convergence criterion of 0.005 eV/Å was used with the Brillouin zone (BZ) sampled by a $12 \times 12 \times 1$ Γ -centered k -point mesh, with a vacuum space of 17 Å adopted along the normal of the lattice plane. To account for the localized nature of the $3d$ electrons of the TM cation a Hubbard correction U is employed within the rotationally invariant approach proposed by Dudarev et al. [32], where $U_{\text{eff}} = U - J$ is the only meaningful parameter. A Hubbard correction of 3 eV and 4 eV is adopted for V_2O_3 and MnBr_3 respectively. The electronic self-consistent calculations were performed with total energy convergence criterion of 10^{-6} eV with the BZ sampled by a denser $24 \times 24 \times 1$ Γ -centered k -point mesh. The atomic structures were visualized by the VESTA program [33].

-
- [1] X. L. Wang. Proposal for a new class of materials: Spin gapless semiconductors. *Phys. Rev. Lett.*, 100:156404, Apr 2008.
 - [2] X. Wang, T. Li, Z. Cheng, X.-L. Wang, and H. Chen. Recent advances in dirac spin-gapless semiconductors. *Applied Physics Reviews*, 5(4):041103, 2018.
 - [3] Motome Y. Ishizuka H. Dirac half-metal in a triangular ferrimagnet. *Phys. Rev. Lett.*, 109:237207, Dec 2012.
 - [4] J. Sun, X. Zhong, W. Cui, J. Shi, J. Hao, M. Xu, and Y. Li. Correction: The intrinsic magnetism, quantum anomalous hall effect and curie temperature in 2d transition metal trihalides. *Phys. Chem. Chem. Phys.*, 22:3128–3128, 2020.
 - [5] J. He, X. Li, P. Lyu, and P. Nachtigall. Near-room-temperature chern insulator and dirac spin-gapless semiconductor: nickel chloride monolayer. *Nanoscale*, 9:2246–2252, 2017.
 - [6] Q. Sun and N. Kioussis. Prediction of manganese trihalides as two-dimensional dirac half-metals. *Phys. Rev. B*, 97:094408, Mar 2018.
 - [7] J.-Y. You, Z. Zhang, B. Gu, and G. Su. Two-dimensional room-temperature ferromagnetic semiconductors with quantum anomalous hall effect. *Phys. Rev. Applied*, 12:024063, Aug 2019.
 - [8] P. Li. Prediction of intrinsic two dimensional ferromagnetism realized quantum anomalous hall effect. *Phys. Chem. Chem. Phys.*, 21:6712–6717, 2019.
 - [9] H. P. Wang, W. Luo, and H. J. Xiang. Prediction of high-temperature quantum anomalous hall effect in two-dimensional transition-metal oxides. *Phys. Rev. B*, 95:125430, Mar 2017.
 - [10] S.-J. Zhang, C.-W. Zhang, S.-F. Zhang, W.-X. Ji, P. Li, P. Wang, S.-S. Li, and S.-S. Yan. Intrinsic dirac half-metal and quantum anomalous hall phase in a hexagonal metal-oxide lattice. *Phys. Rev. B*, 96:205433, Nov 2017.
 - [11] L. Zhang, C.-W. Zhang, S.-F. Zhang, W.-X. Ji, P. Li, and P. Wang. Two-dimensional honeycomb-kagome ta_2s_3 : a promising single-spin dirac fermion and quantum anomalous hall insulator with half-metallic edge states. *Nanoscale*, 11:5666–5673, 2019.
 - [12] C. L. Kane and E. J. Mele. Quantum spin hall effect in graphene. *Phys. Rev. Lett.*, 95:226801, Nov 2005.
 - [13] S. Rachel and K. Le Hur. Topological insulators and mott physics from the hubbard interaction. *Phys. Rev. B*, 82:075106, Aug 2010.
 - [14] C. Griset and C. Xu. Phase diagram of the kane-mele-hubbard model. *Phys. Rev. B*, 85:045123, Jan 2012.
 - [15] M. Hohenadler, T. C. Lang, and F. F. Assaad. Correlation effects in quantum spin-hall insulators: A quantum monte carlo study. *Phys. Rev. Lett.*, 106:100403, Mar 2011.
 - [16] A. Mishra and S. Lee. Magnetic chern insulators in a monolayer of transition metal trichalcogenides. *Scientific Reports*, 8(1):799, 2018.

- [17] M.-H. Whangbo, E.E. Gordon, H. Xiang, H.-J. Koo, and C. Lee. Prediction of spin orientations in terms of homo-lumo interactions using spin-orbit coupling as perturbation. *Accounts of Chemical Research*, 48(12):3080–3087, Dec 2015.
- [18] G. Murthy, E. Shimshoni, R. Shankar, and H. A. Fertig. Quarter-filled honeycomb lattice with a quantized hall conductance. *Phys. Rev. B*, 85:073103, Feb 2012.
- [19] Z. Liu, J. Wang, and J. Li. Dirac cones in two-dimensional systems: from hexagonal to square lattices. *Phys. Chem. Chem. Phys.*, 15:18855–18862, 2013.
- [20] C.-C. Liu, S. Guan, Z. Song, S. A. Yang, J. Yang, and Y. Yao. Low-energy effective hamiltonian for giant-gap quantum spin hall insulators in honeycomb x -hydride/halide ($x = \text{N} - \text{Bi}$) monolayers. *Phys. Rev. B*, 90:085431, Aug 2014.
- [21] G.-F. Zhang, Y. Li, and C. Wu. Honeycomb lattice with multiorbital structure: Topological and quantum anomalous hall insulators with large gaps. *Phys. Rev. B*, 90:075114, Aug 2014.
- [22] C. Wu and S. Das Sarma. $p_{x,y}$ -orbital counterpart of graphene: Cold atoms in the honeycomb optical lattice. *Phys. Rev. B*, 77:235107, Jun 2008.
- [23] C. Wu, D. Bergman, L. Balents, and S. Das Sarma. Flat bands and wigner crystallization in the honeycomb optical lattice. *Phys. Rev. Lett.*, 99:070401, Aug 2007.
- [24] W.-C. Lee, C. Wu, and S. Das Sarma. f -wave pairing of cold atoms in optical lattices. *Phys. Rev. A*, 82:053611, Nov 2010.
- [25] M. Houssa, A Dimoulas, and A Molle. Silicene: a review of recent experimental and theoretical investigations. *Journal of Physics: Condensed Matter*, 27(25):253002, 2015.
- [26] M. Houssa, V.V. Afanasiev, and A. Stesmans. *Structural, Electronic and Transport Properties of Silicene and Germanene*, pages 331–348. 04 2016.
- [27] M. Houssa, B. van den Broek, K. Iordanidou, A.K.A. Lu, G. Pourtois, J.-P. Locquet, V. Afanasiev, and A. Stesmans. Topological to trivial insulating phase transition in stanene. *Nano Research*, 9(3):774–778, 2016.
- [28] A. Molle, J. Goldberger, M. Houssa, Y. Xu, S.-C. Zhang, and D. Akinwande. Buckled two-dimensional xene sheets. *Nature Materials*, 16(2):163–169, 2017.
- [29] G. Kresse and J. Furthmüller. Efficient iterative schemes for ab initio total-energy calculations using a plane-wave basis set. *Phys. Rev. B*, 54:11169–11186, Oct 1996.
- [30] J. P. Perdew, K. Burke, and M. Ernzerhof. Generalized gradient approximation made simple. *Phys. Rev. Lett.*, 77:3865–3868, Oct 1996.
- [31] G. Kresse and D. Joubert. From ultrasoft pseudopotentials to the projector augmented-wave method. *Phys. Rev. B*, 59:1758–1775, Jan 1999.
- [32] S. L. Dudarev, G. A. Botton, S. Y. Savrasov, C. J. Humphreys, and A. P. Sutton. Electron-energy-loss spectra and the structural stability of nickel oxide: An lsda+u study. *Phys. Rev. B*, 57:1505–1509, Jan 1998.
- [33] K. Momma and F. Izumi. *VESTA* for three-dimensional visualization of crystal, volumetric and morphology data. *Journal of Applied Crystallography*, 44(6):1272–1276, Dec 2011.